

Thermal properties of hot-pressed aluminum nitride–graphene composites

Paweł Rutkowski¹ · Dariusz Kata¹ · Kamil Jankowski¹ · Wojciech Piekarczyk¹

Received: 23 June 2015 / Accepted: 9 October 2015 / Published online: 26 October 2015
© The Author(s) 2015. This article is published with open access at Springerlink.com

Abstract This paper concerns the modification of thermal properties of aluminum nitride polycrystalline ceramic material with high thermal conductivity coefficient. The way to change these properties was to distribute graphene particles in the high-conductive matrix. The composite material was hot-pressed at 1900 °C under 25 MPa pressure. The applied pressure allowed to orient the graphene particles and obtain an anisotropy of thermal conductivity. The microstructural observations were made by SEM method. The phases of the matrix were analyzed by XRD measurements, and the existence of graphene was confirmed by Raman spectroscopy. The quantity of graphene in the material after hot-pressing process was determined by thermogravimetric examinations in air flow. The thermal phase stability was checked by differential scanning calorimetry with mass change record. The thermal expansion coefficient was measured by dilatometric method. The thermal diffusivity and thermal conductivity were measured in various directions of the material. The results showed that the anisotropy of thermal conductivity exceeds 100 % for material with 10 mass% of graphene (GPLs). The introduced 2D particles caused a decrease of this parameter in the parallel direction to the load applied during the hot-pressing process.

Keywords Aluminum nitride · Graphene · Microstructure · Thermal stability · Thermal conductivity

Introduction

Aluminum nitride as monocristallic form shows thermal conductivity around $320 \text{ W m}^{-1} \text{ K}^{-1}$ [1]. This value for the aluminum nitride polycrystalline material strongly depends of density [2], grain size [3, 4] and point defects [5, 6]. In order to obtain high thermal conductivity, the sintering additive such as Y_2O_3 , CaO , Yb_2O_3 , and Sm_2O_3 , is required [7–9]. In the air, aluminum nitride powder undergoes an oxidation which leads to forming aluminum oxide covering AlN grains. During the sintering process, yttria reacts with alumina creating liquid phases: YAP (YAlO_3), YAG ($\text{Y}_3\text{Al}_5\text{O}_{12}$), and YAM ($\text{Y}_4\text{Al}_2\text{O}_9$), which leads to the removal of oxygen from the structure of aluminum nitride [10]. Also a type of densification technique of polycrystalline AlN obtaining is very important. The higher the pressure and the higher the heating rate (SPS method), the lower the grain size is, which results in lower thermal conductivity [11, 12]. The use of pressureless sintering with low heating rate and an activator addition allows to obtain large grains with low oxygen contamination in the material [4]. This way, sintered material shows thermal conductivity even equal to 270 °C [13].

Besides its high thermal conductivity coefficient, aluminum nitride is a broadband semiconductor with 6.2 eV band gap [14]. These properties are a main reason of AlN application in electronics, as elements of radars, in productions of light-emitting diodes [15–18].

There is a possibility of modifying thermal conductivity by use of graphene powder and unidirectional pressing process (during hot-pressing process). The use of graphene requires pressure techniques, which allows to change a direction of heat flow in the dense materials. The use of hot-pressing process with uniaxial load results in orientation of graphene in the material in perpendicular direction

✉ Paweł Rutkowski
pawelr@agh.edu.pl; Pawel.Rutkowski@agh.edu.pl

¹ Faculty of Material Science and Ceramics, AGH University of Science and Technology, al. Mickiewicza 30, 30-059 Kraków, Poland

to pressing axis. This behavior was earlier observed by the author of this work in case of Si_3N_4 and Al_2O_3 matrix composites [19–21]. The addition of graphene to the oxide or nitride matrix will cause a decrease in electrical resistivity, which was earlier recorded by the author of this publication in the preliminary electrical measurements of alumina and silicon nitride matrix composites.

The goal of this research was to obtain the aluminum nitride dense material with directed heat flow. To do that, the graphene powder was added to the matrix and the mixture was hot-pressed. The use of HP process with applied uniaxial pressure was supposed to orient graphene particles in the matrix [16, 19]. The microstructural observations and ultrasonic measurements were made to check the anisotropy of such composite material. The influence of the material anisotropy was compared with thermal diffusivity and thermal conductivity measurement made in different material directions. For future possible applications, the thermal stability in air of such composites was checked by DSC/TG method.

Preparation

The commercial aluminum nitride powder of H.C. Starck (grade C) as the matrix, yttria as sintering activator of H.C. Starck (grade C), and graphene Gn(8) of Graphene Laboratories, Inc, USA were used. The size of AlN and Y_2O_3 particles was 3.5 and 1.3 μm , respectively. The graphene (GPLs-graphene platelets) characterization is as follows: color black, purity 99.9 %, average flake thickness 8 nm (20–30 monolayers), average particle (lateral) size $\sim 0.5 \mu\text{m}$ (0.15–3.0), and specific surface area $100 \text{ m}^2\text{g}^{-1}$. Each experimental mixture consisted of 5 mass% of yttrium oxide to improve the sintering process. The amount of graphene in samples was 0, 2, 4, 6, 8, and 10 mass%, respectively.

The powders were mixed in 2-propanol using laboratory rotational dissolver model TD 100 (Pendraulik-Teja) till graphene agglomerates were broken down. As a next step, the mixture was dried out in a vacuum dryer, at a temperature of 90 $^\circ\text{C}$ till constant mass. Dried and granulated powders were hot-pressed (Thermal Technology LLC) at 1900 $^\circ\text{C}$ for 2 h under 25 MPa in nitrogen flow. The heating rate was 10 $^\circ\text{C}$ per min. Sintered bodies with a diameter of 25 mm were obtained. The scheme of mixture in the mold of hot-press is presented in Fig. 1.

Examination route

Apparent density of the sintered samples was calculated using the Archimedes method. The phase composition of the sinters was checked by XRD diffraction (production of Philips with X-Pert HighScore software) and the Rietveld

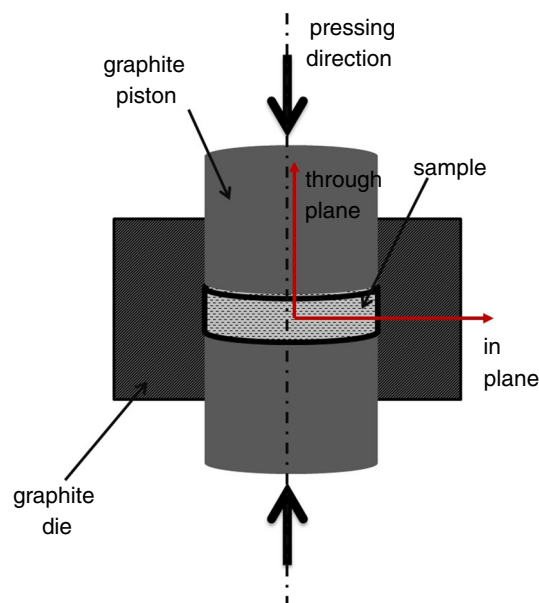


Fig. 1 Scheme of manufacturing hot-pressing process

refinement determining the phase content quantitatively. Raman spectroscopy (Horriba Yvon Jobin LabRAM HR) was used for graphene phase identification. The morphology of samples was observed using the SEM technique—FEI Nova Nano SEM.

The anisotropy of elastic wave velocity was measured by ultrasonic method using UZP-1 (INCO—VERITAS) apparatus.

The thermal stability was measured in the air flow by means of thermogravimetric TG measurements using STA 449 F3 Jupiter[®]. The measurement was made up to temperature of 1000 $^\circ\text{C}$.

Heat measurements were performed on Netzsch LFA 427 apparatus. To determine the specific heat by comparative method, Pyroceram 9606 reference material, with the known coefficient of thermal expansion and specific heat, was used. Thermal diffusivity was determined using the laser pulse method (LFA) for the reference and test material at temperatures ranging from 25 to 300 $^\circ\text{C}$ in the argon flow. The sintered bodies were measured in pressing direction (the direction of applied pressure during manufacturing process) using the “Cape-Lehmann + pulse correction” computational model and in perpendicular direction to the applied pressure using “Radiation + pulse correction” model. At each temperature, three measurements were performed for statistical purposes. Examination of tested materials density changes as a function of temperature in the range up to 300 $^\circ\text{C}$ was performed by determining the coefficient of thermal expansion using a Netzsch DIL 402C dilatometer. Based on these measurements, specific heat was determined using the following formula:

$$c_p^{\text{sample}} = \frac{T_{\infty}^{\text{ref}}}{T_{\infty}^{\text{sample}}} \cdot \frac{Q^{\text{sample}}}{Q^{\text{ref}}} \cdot \frac{V^{\text{sample}}}{V^{\text{ref}}} \cdot \frac{\rho^{\text{ref}}}{\rho^{\text{sample}}} \cdot \frac{D^{\text{ref}}}{D^{\text{sample}}} \cdot \frac{d_{\infty, \text{sample}}^2}{d_{\infty, \text{ref}}^2} \cdot c_p^{\text{ref}} \quad (1)$$

where c_p , specific heat versus temperature of the sample/reference/ $\text{J g}^{-1} \text{K}^{-1}\text{m}$; T , temperature of the sample/reference/ K ; Q , energy absorbed by the sample/reference/ J ; V , amplitude of signal gain for the sample/reference; ρ , apparent density of the sample/reference/ g cm^{-3} ; D , thickness of the test material/ mm ; d , diameter of the measuring aperture of the sample/reference/ mm .

Thermal conductivity was calculated using equation:

$$\lambda(T) = a(T) \cdot c_p(T) \cdot \rho(T) \quad (2)$$

where $a(T)$, thermal diffusivity/ $\text{mm}^2 \text{s}^{-1}$; $c_p(T)$, specific heat/ $\text{J g}^{-1} \text{K}^{-1}$; $\rho(T)$, density of the material/ g cm^{-3} .

The anisotropy of thermal properties was measured using following equation:

$$A = \frac{\lambda_{\text{par}} - \lambda_{\text{per}}}{\lambda_{\text{par}}} \times 100 \% \quad (3)$$

where λ_{par} , thermal conductivity in parallel direction to pressing axis, through plane direction/ $\text{W m}^{-1} \text{K}^{-1}$; λ_{per} ,

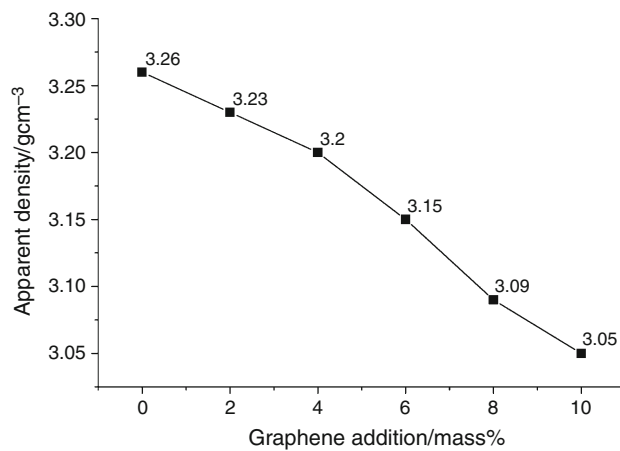


Fig. 2 Density changes of hot-pressed aluminum nitride-graphene composites

thermal conductivity in perpendicular direction to pressing axis, in plane direction/ $\text{W m}^{-1} \text{K}^{-1}$.

Results and discussion

The apparent density of the AlN-graphene composites, measured by hydrostatic method, is shown in Fig. 2. The density is falling down with an increase in graphene content. The relative density of the hot-pressed materials is above 99 % Table 1.

The XRD qualitative phase measurements supported by quantitative Rietveld analysis showed the existence of YAG phase and YAP in the composites (Table 1). The YAP phase exists only in the case of composite with 4 mass% graphene additive. For the rest of the composite, the YAG phases increase with graphene addition. The phase analysis indicates on graphite phase rising with graphene initial content.

The Raman spectroscopy, presented in Fig. 3, confirm, the existence of graphene phase in the composites. The spectrum of the measured materials covers with wavenumber of the pure graphene powder: 3243, 2727, 1578, and 1349 cm^{-1} . The magnification of the band at

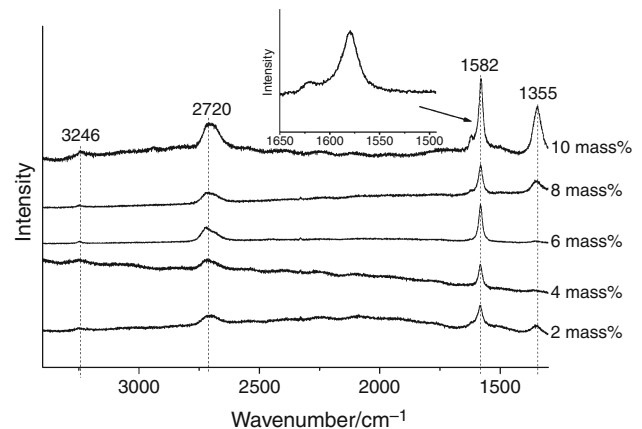


Fig. 3 Raman spectra of hot-pressed aluminum nitride-graphene composites

Table 1 Phase analysis of hot-pressed aluminum nitride-graphene composites

Measured material	Relative density/%	Phase composition/mass%			
		AlN	YAG	YAP	Graphite
0 mass% Gn(8)	98.7	96.1	3.9	0	0
2 mass% Gn(8)	99.0	94.5	5.1	0	0.4
4 mass% Gn(8)	99.9	96.7	0	2.2	1.0
6 mass% Gn(8)	99.5	90.4	7.9	0	1.6
8 mass% Gn(8)	99.5	90.2	7.6	0	2.2
10 mass% Gn(8)	99.4	88.4	8.6	0	3.0

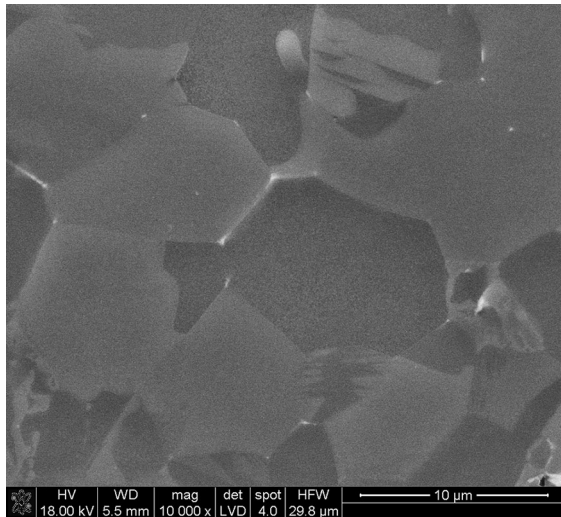


Fig. 4 SEM observations of AlN + 5 mass% Y_2O_3

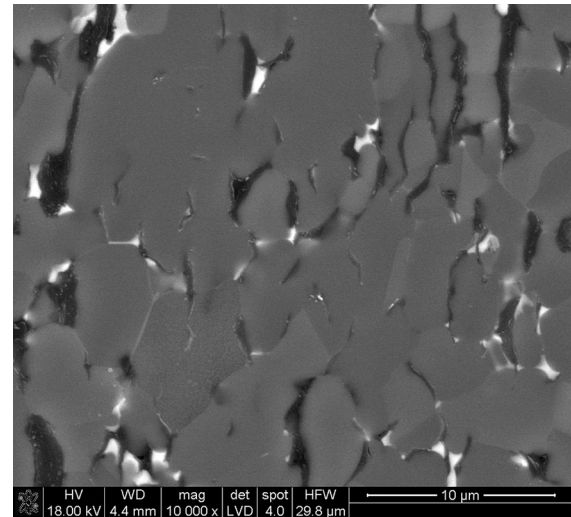


Fig. 6 SEM observations of AlN + 5 mass% Y_2O_3 + 6 mass% Gn(8)

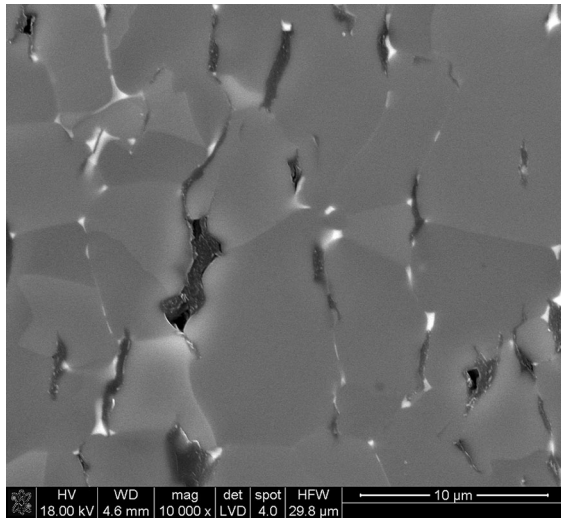


Fig. 5 SEM observations of AlN + 5 mass% Y_2O_3 + 2 mass% Gn(8)

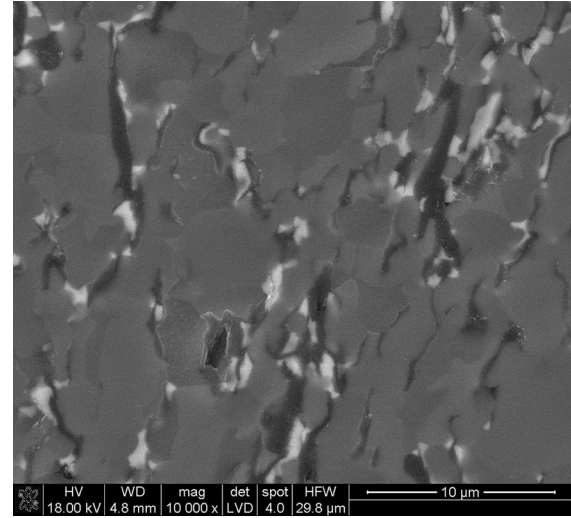


Fig. 7 SEM observations of AlN + 5 mass% Y_2O_3 + 10 mass% Gn(8)

around 1600 cm^{-1} wavenumber indicates that the ratio of G (1582)/D' (1620) is decreasing, which confirms graphene defects [22, 23]. An increase in D2 (2720), in comparison with G (1582) band, shows a rising number of graphene layers.

The microstructural observations were made on the polished surfaces. The examples of the results for different graphene content are illustrated in Figs. 4–7.

The examples of microstructural observations, made on aluminum nitride–graphene composites show that the addition of GPLs to the material leads to a decrease in grain size of the matrix. The flakes of the introduced graphene flakes are oriented in the perpendicular direction to the load applied during the hot-pressing process. The similar situation was observed by the author of this work in

case of composites with silicon nitride and alumina matrix [20, 21]. There are visible large graphene inclusions in AlN matrix, which are the “agglomerates” of graphene flakes. The white phase is YAG or YAP coming from the yttria and alumina (covering AlN grains) reaction.

The graphene orientation, observed in the composites microstructure, was investigated by ultrasonic measurement of longitudinal wave velocity. The recorded wave velocity versus graphene content in different directions is presented in Fig. 8. Figure 9 illustrates the anisotropy calculated from ultrasonic measurements' data. The results of the ultrasonic examination show that the anisotropy can reach even 30 % in case of 8 % graphene addition. The measurements and the microstructural

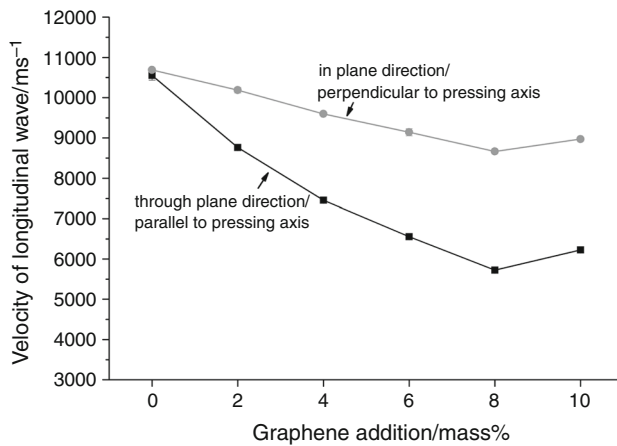


Fig. 8 Longitudinal wave velocity versus material direction of hot-pressed aluminum nitride-graphene Gn(8) composites

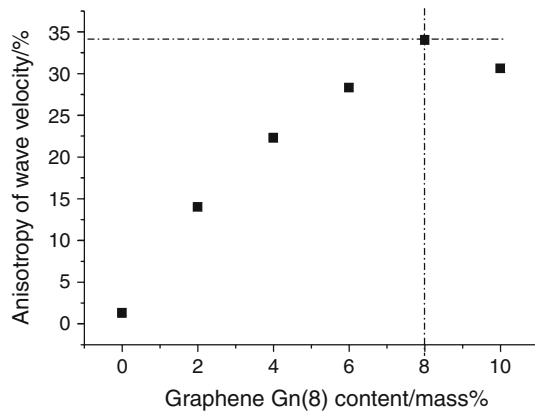


Fig. 9 Anisotropy of longitudinal wave velocity of hot-pressed aluminum nitride-graphene Gn(8) composites

observations confirmed the graphene orientation in the material (Figs. 5–7).

Because of the standard working conditions of aluminum nitride parts, which are in the air atmosphere, the AlN-Gn(8) materials were tested by differential scanning calorimetry (DSC) with mass control (TG). The stability of obtained composites versus graphene content is illustrated by DSC signal in Fig. 8 and TG signal in Fig. 9. The recorded data show that pure aluminum nitride is thermally

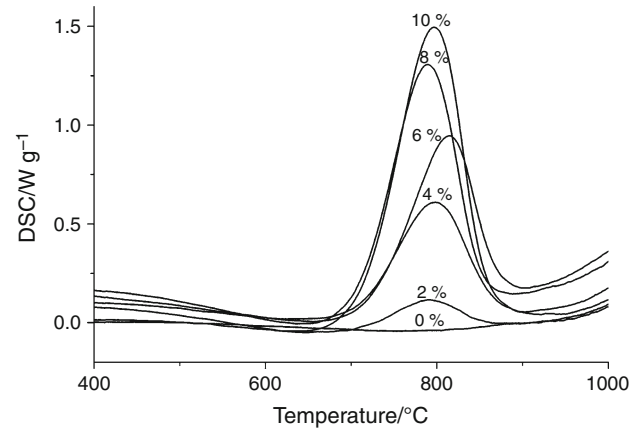


Fig. 10 Thermal stability, DSC signal of hot-pressed aluminum nitride-graphene Gn(8) composites

stable up to 1000 °C. The composites can work safely up to 650 °C. The oxidation onset is in the range of 710–730 °C and endset is about 860 °C (Table 2). The maximum of the exothermic signal if the oxidation process is around 800 °C. Additionally, the mass change measurements (Table 2), made in the air, allow to calculate the graphene content in the composites and furthermore the relative density, which was not possible with the use of XRD/Rietveld data (Fig. 10). The relative density is collected in Table 1. The oxidation reaction heat increases with the content of graphene starting from 70 J g⁻¹ and reaching 810 J g⁻¹ for 10 mass% of introduced GPLs (Table 2).

Thermal conductivity depends on anisotropy of the microstructure in the material because of used manufacturing technology and flakes of graphene (Figs. 11, 12). The calculated thermal conductivity versus temperature, made on the base of diffusivity measurements, is illustrated in Figs. 13 and 14. The comparison of the thermal conductivity, made in different material directions at room temperature, is presented in Fig. 12. The thermal diffusivity at room temperature in different directions and the calculated anisotropy are presented in Table 4.

The thermal expansion coefficient (TEC) measurements results, which are required for calculation of thermal conductivity, are listed in Table 3 (for different material

Table 2 Analysis of DSC signal after oxidation process of AlN-GPLs composites

Graphene addition/mass%	Area/J g ⁻¹	Peak/°C	Onset/°C	Endset/°C	Height/W g ⁻¹	Width/°C	Mass loss/%
2	69.2	791.0	732.5	850.7	0.14	96.5	0.8
4	340.4	798.3	718.5	863.9	0.58	109.8	3.3
6	443.1	814.7	728.3	865.1	0.83	99.8	5.7
8	655.7	788.3	712.4	848.0	1.22	100.1	7.7
10	810.7	796.9	715.8	852.6	1.48	101.7	9.3

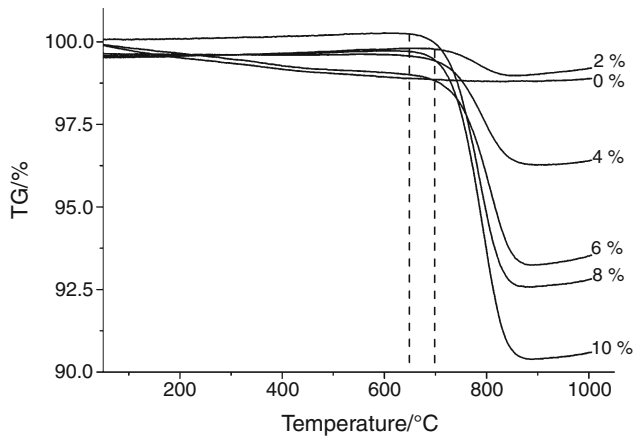


Fig. 11 Thermal stability, TG signal of hot-pressed aluminum nitride-graphene Gn(8) composites

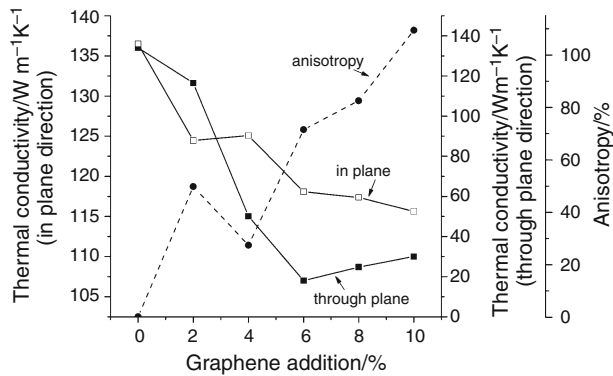


Fig. 12 Thermal conductivity and its anisotropy at room temperature of hot-pressed aluminum nitride-graphene Gn(8) composites versus measurement direction

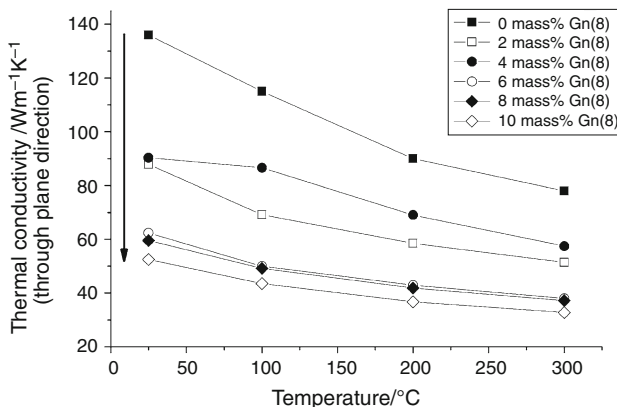


Fig. 13 Thermal conductivity versus temperature of hot-pressed aluminum nitride-graphene Gn(8) composites, in pressing direction/through plane

directions). The results of TEC show that the graphene particles and used densification technology do not have significant influence on this parameter, neither versus

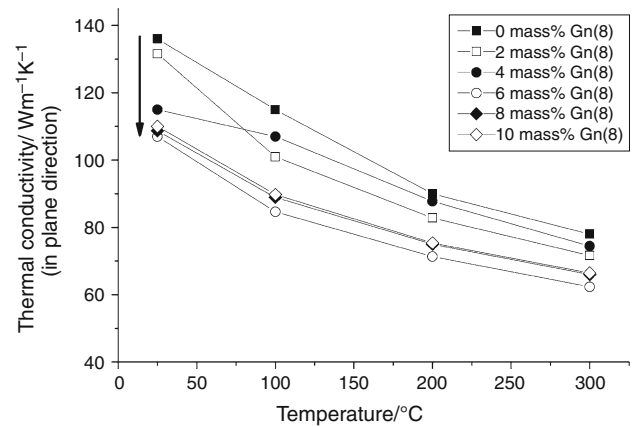


Fig. 14 Thermal conductivity versus temperature of hot-pressed aluminum nitride-graphene Gn(8) composites, perpendicular pressing direction/in plane

Table 3 Thermal expansion coefficient versus graphene addition

HP	
Sample	CTE·10 ⁻⁶ /°C ⁻¹
0 mass% Gn(8)	4.4
2 mass% Gn(8) parallel	4.8
4 mass% Gn(8) parallel	4.6
6 mass% Gn(8) parallel	5.1
6 mass% Gn(8) perpendicular	5.4
8 mass% Gn(8) parallel	5.2
8 mass% Gn(8) perpendicular	4.9
10 mass% Gn(8) parallel	5.4
10 mass% Gn(8) perpendicular	5.2

graphene content nor measurement direction. The TEC is in the range of $4.6\text{--}4.8 \cdot 10^{-6} \text{ }^{\circ}\text{C}^{-1}$.

Data collected on the base of laser flash analysis method (Table 4) show that the graphene content and a decrease in grain size of the matrix (probably caused by graphene addition) lower the value of thermal diffusivity in both of material directions. The decrease in this parameter is stronger in parallel direction (through plane—Fig. 1) to applied pressure (during PH process) than for perpendicular one (in plane, in direction of graphene flakes). This anisotropy reaches almost 110 % for 10 mass% of GPLs content (Table 4). It is a result of graphene orientation formed during the hot-pressing process.

The results of thermal conductivity presented in Fig. 12 show that the parameter decreases with graphene addition and with the grain size in both directions, which is in accordance with thermal diffusivity (direct measured result). The calculated parameter is higher in graphene flakes direction (oriented, microstructure in Fig. 7) than in

Table 4 Thermal diffusivity of aluminum nitride–graphene Gn(8) composites

Graphene addition	Pressing method	Thermal diffusivity in parallel direction/mm ² s ⁻¹	Thermal diffusivity in perpendicular direction/mm ² s ⁻¹	Anisotropy/ % (in comparison to parallel direction)
0 mass% Gn(8)	HP	56.25 ± 0.20	56.25 ± 0.20	–
2 mass% Gn(8)	HP	33.01 ± 0.10	49.45 ± 0.72	49.8
4 mass% Gn(8)	HP	27.46 ± 0.45	41.68 ± 0.17	51.8
6 mass% Gn(8)	HP	23.89 ± 0.10	40.96 ± 0.20	71.5
8 mass% Gn(8)	HP	21.22 ± 0.08	38.73 ± 0.02	82.5
10 mass% Gn(8)	HP	18.95 ± 0.01	39.73 ± 0.10	109.7

the pressing axis. The anisotropy of conductivity exceeds 100 %. For 4 mass% of GPLs, the anisotropy decreases, which can be partly connected with small quantity of YAP phase formation instead of YAG one. The thermal conductivity results in higher temperature (about 300 °C) show that in the pressing axis (through plane) this property decreases strongly with GPLs content. For 10 mass% of GPLs, this value reaches around 40 W m⁻¹ K⁻¹, which is 50 % of the pure polycrystalline aluminum nitride (reference one). In the perpendicular direction, the decrease in thermal conductivity is much lower and the value is above 60 W m⁻¹ K⁻¹ at 300 °C. In accordance with Eq. 2, the falling down apparent density will cause a decrease in thermal conductivity of the materials. Looking at the relative density (Table 1) the small content of porosity, mostly in the GPLs agglomerates, can be a partial reason for the thermal diffusivity/conductivity decrease.

Conclusions

The dense AlN–graphene (GPLs) materials were obtained by hot-pressing method. The applied uniaxial pressure (during HP process) resulted in graphene orientation in the composites. Also the increasing GPLs content caused decreasing in grain size of the matrix. Such microstructure had an influence on thermal properties of the composites. The lowering grain size of AlN in combination with graphene particles oriented in perpendicular direction to applied pressure resulted in high anisotropy of thermal diffusivity and thermal conductivity. Probably the decreasing grain size of the matrix was the reason for lowering thermal properties in both directions of the material. The orientation of graphene flakes allowed to obtain higher thermal conductivity in perpendicular direction to applied pressure (so in plane/in flake direction). The higher the graphene content, the higher the anisotropy of heat flow in the composites.

Acknowledgements The study constitutes a part of the project no. GRAFTECH/NCBR/03/05/2012 “Ceramic composites with graphene content as cutting tools and device parts with unique properties” and in case of the material preparation as a part of TERMET project “New Construction Materials with High Thermal Conductivity”. Results supported by the National Centre for Research and Development (Poland).

Open Access This article is distributed under the terms of the Creative Commons Attribution 4.0 International License (<http://creativecommons.org/licenses/by/4.0/>), which permits unrestricted use, distribution, and reproduction in any medium, provided you give appropriate credit to the original author(s) and the source, provide a link to the Creative Commons license, and indicate if changes were made.

References

1. Watari K, Ceramics High thermal conductivity non-oxide. *J Ceram Soc Jpn.* 2001;109:S7–16.
2. Slack GA. Nonmetallic crystals with high thermal conductivity. *J Phys Chem Solids.* 1973;23:321–35.
3. Qiao L, Zhou H, Chen K, Fu R. Effects of Li₂O on the low temperature sintering and thermal conductivity of AlN ceramics. *J Eur Ceram Soc.* 2003;23:1517–24.
4. Bellosi A, Esposito L, Scafe E, Fabbri L. The influence of microstructure on the thermal conductivity of aluminum nitride. *J Mater Sci.* 1994;29:5014–22.
5. Sakuma K, Okada A, Kawamoto H. Effects of cation impurities on thermal conductivity of yttria-doped aluminum nitride. *J Mater Synth Process.* 1998;6:315–21.
6. Medraj M, Baik Y, Thompson WT. Understanding AlN sintering through computational thermodynamics combined with experimental investigation. *J Mater Process Tech.* 2005;161:415–22.
7. Heping Z, Yaocheng L, Weiguo M, Yin W. Effects of binary additives B₂O₃–Y₂O₃ on the microstructure and thermal conductivity of aluminum nitride ceramics. *J Mater Sci.* 1999;34:6165–8.
8. Geith A, Kulig M, Hofmann T, Rüssel C. Thermal conductivity of calcium-doped aluminium nitride ceramics. *J Mater Sci.* 1993; 28:865–9.
9. Jackson B, Virkar A. High-thermal-conductivity aluminum nitride ceramics: the effect of thermodynamic, kinetic, and microstructural factors. *J Am Ceram Soc.* 1997;80:1421–35.
10. Medraj M, Hammond R, Parvez MA, Drew RAL, Thompson WT. High temperature neutron diffraction study of the Al₂O₃–Y₂O₃ system. *J Eur Ceram Soc.* 2006;26:3515–24.

11. Li MJ, Zhang LM, Shen Q, Li T. Microstructure and properties of spark plasma sintered AlN ceramics. *J Mater Sci.* 2006;41:7934–8.
12. Rutkowski P, Kata D. Thermal properties of AlN polycrystals obtained by pulse plasma sintering method. *J Adv Ceram.* 2013;2:180–4.
13. Kuramoto N, Taniguchi H, Aso I. Development of translucent aluminum nitride ceramics. *Am Ceram Soc Bull.* 1989;68:883–6.
14. Molony B. Technology and investment. Cambridge: Harvard College; 1990.
15. Tieg TN, Kiggans Jr, James O. High thermal conductivity lossy dielectric using codensified multilayer configuration, assignee: Lockheed martin energy research corporation. U.S. Patent Mo. 6,579393. 2003.
16. Baik K, Drew RAL. Aluminum nitride: processing and applications. *Key Eng Mat.* 1996;122–124:553–70.
17. Harris J. Sintered aluminum nitride ceramics for high-power electronic applications. *JOM.* 1998;50:56–60.
18. Taniyasu Y, et al. An aluminium nitride light-emitting diode with a wavelength of 2010 nanometres. *Nature.* 2006;441:325–8.
19. Rutkowski P, Stobierski L, Zientara D, Jaworska L, Klimczyk P, Urbanik M. The influence of the graphene additive on mechanical properties and wear of hot-pressed Si₃N₄ matrix composites. *J Eur Ceram Soc.* 2015;35:87–94.
20. Rutkowski P, Stobierski L, Górny G. Thermal stability and conductivity of hot-pressed Si₃N₄-graphene composites. *J Therm Anal Calorim.* 2014;116:321–8.
21. Rutkowski P, Klimczyk P, Jaworska L, Stobierski L, Dubiel A. Thermal properties of pressure sintered alumina-graphene composites. *J Therm Anal Calorim.* 2015;. doi:[10.1007/s10973-015-4694-x](https://doi.org/10.1007/s10973-015-4694-x).
22. Yan Z, Barron AR. Characterization of Graphene by Raman Spectroscopy. http://cnx.org/contents/f06226c5-c2a4-4798-9c75-b016acea73cd@3/Characterization_of_Graphene_b.
23. Sitarz M, Czosnek C, Jeleń P, Odziomek M, Olejniczak Z, Kozanecki M, Janik JF. SiOC glasses produced from silsesquioxanes by the aerosol-assisted vapor synthesis method. *Spectrochim Acta A.* 2013;112:440–5.